Supplemental material for: Superfluid Fraction of a 2D Bose-Einstein Condensate in a Triangular Lattice

F. Rabec, G. Brochier, S. Wattellier, G. Chauveau, Y. Li, S. Nascimbene, J. Dalibard, J. Beugnon*
Laboratoire Kastler Brossel, Collège de France, CNRS, ENS-PSL University, Sorbonne Université, 11 Place Marcelin Berthelot, 75005 Paris, France
(Dated: February 27, 2026)

Determination of the compressibility

We detail in this paragraph the determination of Eq. (7) of the main text. In the presence of a periodic potential $V(\boldsymbol{r})$, the GPE for the many-body wave function $\psi(\boldsymbol{r})$ reads

$$-\frac{\hbar^2}{2M}\boldsymbol{\nabla}^2\psi(\boldsymbol{r}) + g|\psi(\boldsymbol{r})|^2\psi(\boldsymbol{r}) + V(\boldsymbol{r})\psi(\boldsymbol{r}) = \mu\psi(\boldsymbol{r}), \tag{1}$$

where μ is the chemical potential and $\int |\psi(\boldsymbol{r})|^2 \mathrm{d}\boldsymbol{r} = N$ for a given atom number N. When an additional force F_y is applied along the y direction, the previous equation is modified by adding a term $-F_y y\psi(\boldsymbol{r})$ to the right-hand side. If, over a unit cell of the potential, the variation of $F_y y$ is much smaller than μ, one can write

$$-\frac{\hbar^2}{2M}\boldsymbol{\nabla}^2\psi(\boldsymbol{r}) + g|\psi(\boldsymbol{r})|^2\psi(\boldsymbol{r}) + V(\boldsymbol{r})\psi(\boldsymbol{r}) = \left(\mu - F_y y_c\right)\psi(\boldsymbol{r}), \tag{2}$$

where y_c is the cell center. Each unit cell thus has a local chemical potential $\mu - F_y y_c$. The mean density over the cell is given by

$$\langle\rho\rangle_{\mathrm{UC}} = \rho_0 - \left.\frac{\partial\rho}{\partial\mu}\right|_\mu F_y y_c = \rho_0\left(1 - \kappa F_y y_c\right), \tag{3}$$

where ρ_0 is the average density over the whole system and κ its compressibility. The CoM displacement induced by the force F_y is given by

$$\delta_y = \frac{1}{N}\iint \mathrm{d}x\mathrm{d}y\, y\,[\rho(x,y) - \rho_0]. \tag{4}$$

We also assume that the system is symmetric with respect to the origin and is periodic with period d along y. Splitting the integration over each unit cell and using Eq. (3), we obtain

$$\delta_y = \frac{\rho_0\kappa F_y L}{N} d \sum_{i=-L/2d}^{L/2d} (id)^2 \simeq \frac{\kappa F_y L^2}{12}. \tag{5}$$

Optical lattice potential generation

The characteristics of the optical system can be found in the Supplemental Material of Ref. [1]. The optical lattice potential imprinted on the atoms is approximately given by Eq. (2) in the main text. To imprint this potential, we display the following profile on the DMD, which acts as an amplitude modulator [2]:

$$f(\boldsymbol{r}) = s(\boldsymbol{r})\sqrt{B - A\sum_{m=0}^{2}\cos(\boldsymbol{k}_m\cdot\boldsymbol{r} + \phi_m)}, \tag{6}$$

where A and B are positive coefficients chosen such that $\forall\boldsymbol{r}$, $f^2(\boldsymbol{r}) \in [0.1, 1]$. A proper choice of the spatial origin allows us to set $\phi_1 = \phi_2 = 0$. We also choose $\Phi = 0$, but imperfections in the optical system imaging the DMD pattern onto the atoms lead to a modified potential with a nonzero value of Φ, calibrated as shown in the next section. The function $s(\boldsymbol{r})$ is determined in a separate calibration experiment to make the laser beam profile reflected off the DMD uniform over the size of the cloud. Since the DMD is a binary amplitude modulator, we obtain a smoothly varying profile following Eq. (6) using a dithering method [2]. The coefficients A and B and the correction function $s(\boldsymbol{r})$ remained constant during data acquisition; the lattice amplitude was tuned by adjusting the power of the light illuminating the DMD.

Optical lattice potential characterization

We use an auxiliary CCD camera, which provides an image of the trapping light profile in the atomic plane, to monitor and calibrate the potential imposed on the cloud. We first compare the measured intensity profile to the one introduced in Eq. (2) of the main text. We fit the data to the following function:

$$\begin{aligned} I(\boldsymbol{r}) = \bar{I} + I_0\cos(\boldsymbol{k}_0\cdot\boldsymbol{r}) + I_1\cos(\boldsymbol{k}_1\cdot\boldsymbol{r}) \\ + I_2\cos(-\boldsymbol{k}_0\cdot\boldsymbol{r} - \boldsymbol{k}_1\cdot\boldsymbol{r} + \Phi), \end{aligned} \tag{7}$$

where the phases in the first two cosines have been set to zero by a proper choice of the spatial origin. We obtain $I_2/I_0 = 1.00(2)$, $I_1/I_0 = 0.98(2)$, $k_1/k_0 = 0.96(1)$, $\Phi = 0.21(1)\pi$, and an angle $\vartheta = 0.671(6)\pi$ between the two vectors $\boldsymbol{k}_0$ and $\boldsymbol{k}_1$. This measurement justifies, within error bars, the choice of potential in Eq. (2) of the main text. For all computations with the GPE shown in this work, we consider the isotropic lattice given in Eq. (2) of the main text with $\Phi = 0.21\pi$.

Calibration of the imaging system and reconstruction of the density profile

As introduced in the main text, the finite imaging resolution of the atomic cloud must be taken into account when we

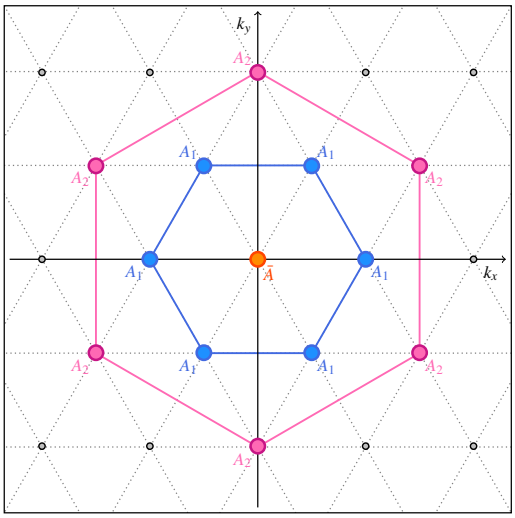

Figure 1. **Fourier components used for fitting the density profile.** We fit the density profiles using a sum of two triangular lattices of different periods and an average density $\bar{A}$. The amplitude of the components of the triangular lattice of period $\lambda_1 = 6\,\mu$m (resp. $\lambda_2 \simeq 3.46\,\mu$m) are all equal to A_1 (resp. A_2) to ensure the isotropy of the deduced superfluid fraction tensor. The norm and orientation of the wave vectors of the lattices are also fixed according to this figure.

determine the superfluid fraction or Leggett bounds from the measured density profile. We write this profile as

$$\rho^{\text{meas}}(\boldsymbol{r}) = \rho_0 + \sum_{n>0} \beta_n \rho_n(\boldsymbol{r}), \tag{8}$$

where the β_n are the attenuation factors associated with a given spatial frequency with index n of the density modulation. We calibrated the β_n using the same method as described in Ref. [1], which we briefly summarize here.

First, we calibrate the light intensity level using the atomic response to a lattice with a large period of 24 µm, for which we can safely assume that the corresponding β coefficient is one. We use shallow lattice potentials so that the induced density modulation $\Delta\rho$ is well approximated by

$$\frac{\Delta\rho}{\rho_0} \approx \frac{V_0}{g\rho_0 + \varepsilon_k/2}, \tag{9}$$

where $\varepsilon_k = \hbar^2 k^2/2M$ is the recoil energy of the triangular lattice of period $4\pi/(\sqrt{3}k)$. We then compare the atomic response for different lattice periods to this reference measurement and obtain $\beta_1 = 0.71(4)$ and $\beta_2 = 0.36(16)$, corresponding to lattice periods of $\lambda_1 = d = 6\,\mu$m and $\lambda_2 \simeq 3.46\,\mu$m, respectively. For smaller periods, the values of the β_n are compatible with zero within error bars.

We determine the superfluid fraction and Leggett bounds from *in situ* images using a reconstructed density profile that we obtain from a fit of the experimental images to a function including the first two spatial frequencies of the triangular lattice and taking into account the correction by the attenuation factors $\beta_{1,2}$ of the imaging system. The fitting function is given by

$$n(\boldsymbol{r}) = \bar{A} + A_1 \sum_{\alpha=0}^{\alpha=2} \cos[\boldsymbol{k}_\alpha^{(1)} \cdot (\boldsymbol{r} - \boldsymbol{r}_0) + \varphi_1] + A_2 \sum_{\gamma=0}^{\gamma=2} \cos[\boldsymbol{k}_\gamma^{(2)} \cdot (\boldsymbol{r} - \boldsymbol{r}_0) + \varphi_2] \tag{10}$$

It corresponds to an average density $\bar{A}$ modulated by the sum of two triangular lattices with period $\lambda_1 = 2\pi/|\boldsymbol{k}_\alpha^{(1)}|$ and $\lambda_2 = 2\pi/|\boldsymbol{k}_\alpha^{(2)}|$. The $\boldsymbol{k}_\alpha^{(1)}$ are defined in Eq. (2) of the main text, and we choose $\boldsymbol{k}_i^{(2)} = \boldsymbol{k}_i^{(1)} - \boldsymbol{k}_{i-1}^{(1)}$ (with circular permutation of the indices). We ensure that this function is invariant under a rotation by an angle of $2\pi/3$ around $\boldsymbol{r}_0$ by imposing the same amplitude $A_{1,2}$, the same norm $|\boldsymbol{k}_{\alpha,\beta}|$, and the expected orientation of the $\boldsymbol{k}_{\alpha,\beta}$ (see Fig. 1) for the three terms of each of the two triangular lattices. The free parameters of the fit are thus $\bar{A}$, A_1, A_2, $\boldsymbol{k}_0^{(1)}$, $\boldsymbol{r}_0$, φ_1 and φ_2.

For the range of parameters explored in this work, $V_0 < 5\,g\rho_0$ and $f_s > 0.4$, we verified numerically that the truncation to the Fourier components show in Fig. 1 is sufficient to provide a robust estimate of these quantities. For large V_0, this truncation is expected to slightly underestimate the f_s^- bound, which is the most sensitive to it. The truncation to these first two Fourier components also leads to an unphysical reconstructed density profile with negative values for sufficiently large potential depth. We address this issue by setting points with negative density values to a small arbitrary nonzero value $\epsilon = 10^{-25}$ after normalizing the profiles to a maximum value of 1. We confirmed numerically that this procedure gives a stable determination of the studied quantities for any sufficiently small value of ϵ.

Potential landscape

We show in Fig. 2 some characteristics of the lattice potential studied in this work. We highlight in Fig. 2a the positions of the minimum and maximum of the potential, as well as the existence of a local maximum and a saddle point. As discussed in the main text, the energy barrier separating two neighboring minima of the potential is smaller than its peak-to-peak amplitude. The potential landscape along a closed triangular trajectory connecting all these particular points is shown in Fig. 2b. Setting the energy of the potential minimum to zero and $A_L = 1$ for simplicity, the energies of the saddle and maximum points are $V_{\text{saddle}} \simeq 3.72$ and $V_{\text{max}} \simeq 4.96$, respectively. We also show the normalized density profile computed with GPE for the largest potential studied in this work. At the saddle point the density is ∼7 % of the maximum density. Finally, we show in Fig. 2c the potential landscape and the associated density profile for a path linking two minima through the saddle point. We also show in Fig. 3, the predicted superfluid fraction when the density profile is computed in the Thomas-Fermi approximation. As expected, the computed superfluid fraction lies below the GPE prediction and

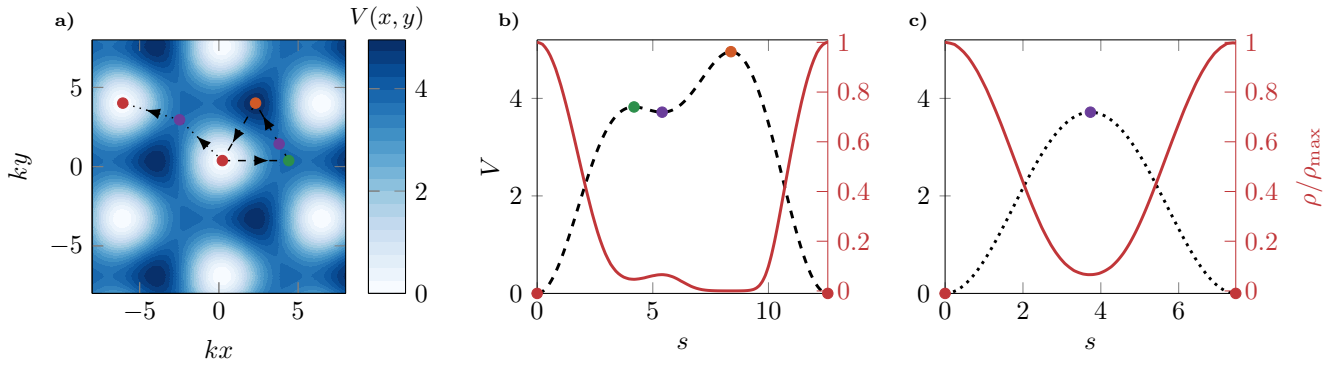

Figure 2. **Potential landscape** (a) 2D profile of the triangular lattice potential for $\Phi = 0.21\pi$ and where we have fixed the potential minimum $V_{\min} = 0$ and $A_L = 1$ for simplicity. The global minimum (red dot), maximum (orange dot, $V_{\max} \simeq 4.96$), local maximum (green dot, $V_{\text{loc}} \simeq 3.83$) and saddle point (violet dot, $V_{\text{saddle}} \simeq 3.72$) have been highlighted. (b) Potential landscape (dashed black line) along the dashed line shown in (a) and corresponding normalized density computed with the GPE (solid red line) for $V_0 = 4.7\, g\rho_0$. The density at the saddle point is ~7 % of the maximum density. (c) Same as in (b) but along the dotted line shown in (a).

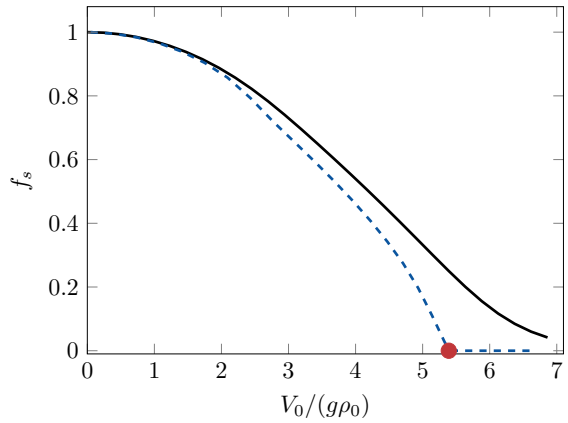

Figure 3. **Superfluid fraction in the Thomas-Fermi approximation.** Superfluid fraction determined for a density profile computed in the Thomas-Fermi approximation (dashed blue line) and with the GPE (solid black line). The red point indicates the predicted potential V_0 at which μ_{TF}, the chemical potential computed in the Thomas-Fermi approximation, equals the saddle point energy, resulting in $f_s = 0$.

reaches zero when the chemical potential of the cloud is equal to the energy of the saddle point at $V_0 \simeq 5.4\, g\rho_0$.

Comparison of Leggett bounds to numerical predictions

We show in Fig. 4 the Leggett bounds computed from the density profile for $\theta = 0, \pi$. These data are in good agreement with the predictions of the GPE (dashed lines).

* beugnon@lkb.ens.fr

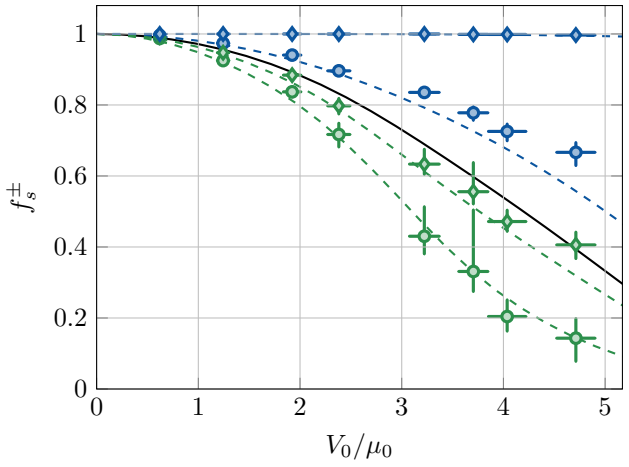

Figure 4. **Leggett bounds.** Measured Leggett bounds corresponding to the upper bounds $f_s^+(\boldsymbol{e_y})$ (blue diamonds) and $f_s^+(\boldsymbol{e_x})$ (blue circles), and to the lower bounds $f_s^-(\boldsymbol{e_y})$ (green diamonds) and $f_s^-(\boldsymbol{e_x})$ (green circles). Error bars correspond to the error propagation of the uncertainties in the calibration of the imaging system response and of the lattice. The dashed lines are the prediction for these bound computed on the profiles obtained from the simulations of the GPE. The solid line is the predicted superfluid fraction.

[1] G. Chauveau, C. Maury, F. Rabec, C. Heintze, G. Brochier, S. Nascimbene, J. Dalibard, J. Beugnon, S. M. Roccuzzo, and S. Stringari, Superfluid fraction in an interacting spatially modulated Bose-Einstein condensate, Phys. Rev. Lett. **130**, 226003 (2023).

[2] C. Dorrer and J. D. Zuegel, Design and analysis of binary beam shapers using error diffusion, J. Opt. Soc. Am. B **24**, 1268 (2007).